Proceedings of the 28th IEEE
EMBS Annual International Conference
New York City, USA, Aug 30-Sept 3, 2006

Characterizing 3-D Geometry of Mouse Aortic Arch Using Light Stereo-Microscopic Imaging

Hui Zhu, Jessica Shih, David S. Long, Nobuyo Maeda, John R. Hagaman, and Morton H. Friedman

Abstract—**The vascular geometry may play an important role in the development of atherosclerosis by modulating the local hemodynamics and mechanical stresses of the vessel wall. The mouse is now the most popular animal model to study cardiovascular disease. Here, we present a method to characterize the 3-D geometry of mouse aortic arches by casting and light stereo-microscopic imaging. After calibration of the stereo-microscopic imaging system, the 3-D axis of an aortic cast is reconstructed using two stereo images. Based on the analysis of this 3-D curve, a geometry-based definition of the arch segment is given, and some geometric features, including curvature, torsion, and symmetry, have been derived. Casts from a C57BL6 and a SVEV mouse have been processed. This method will be used to detect the geometric difference of the aortic arch among different mouse strains.**

I. Introduction

Cardiovascular disease is still the No. 1 cause for mortality of Americans [1]. Besides the traditionally identified risk factors, such as hypercholesterolemia, hypertension, smoking, diabetes, and gender, there is ample evidence that vessel wall mechanics and hemodynamics may play an important role in atherosclerosis [2-5]. From fundamental mechanics, both the fluid dynamics in the vessel and the stress distribution in the vessel wall are dependent on the vessel geometry. Therefore, it is plausible that some geometric features may affect the course of atherosclerosis in the vessel through their influence on the local mechanical environment, which would be "geometric risk factors".

To study "geometric risk factors" based only on human subjects is difficult due to the unavailability of non-invasive observational approaches and in vivo histological and genetic techniques, let alone patient availability, risks and costs. For almost a century, animals, including avian, rodents, rabbits, dogs, swine, and nonhuman primates, have been used as experimental models in studying atherosclerosis [6]. However, few of these studies focused on vascular geometry. Over the last decade, the mouse has become the predominant species to study atherosclerosis [7, 8], owing to the availability of knockouts that demonstrate rapid development of human-like vascular disease, pure strains that can be used to probe heritability of disease, and the relatively low experimental cost. The small size of mice facilitates the use of large group numbers that can be maintained in highly controlled environments when studying a specific atherogenic mechanism.

Although there are a few micro-imaging techniques that have the capability to directly view the geometry of the mouse vessels, such as magnetic resonance imaging (MRI) [9], and microangiography [10, 11], the imaging cost is still very high relative to the cost of the animals. Light stereo-microscopic imaging (LSMI) is an inexpensive technique for the three-dimensional (3-D) reconstruction of micro-scale objects based on the two-view vision theory [12]. This reconstruction technique has been widely applied in biplane angiography to reconstruct coronary arteries in 3-D [13-16].

The aortic arch is often selected to study atherosclerosis in mice, because this area is very susceptible to the disease. In this paper, we use LSMI to reconstruct 3-D axes of mouse aortic arches from their casts, and obtain several geometric parameters based on the 3-D axis curve. The geometric features between two common used mouse strains, C57BL6 and SVEV, are compared. Section II is a brief summary of the cast preparation. Our LSMI system, and the system calibration and 3-D reconstruction algorithms are presented in Section III, as well as the geometric features extracted from the cast axis. Results are shown in Section IV. Section V is the conclusion.

Fig. 1. The aortic cast from the C57BL6 mouse.

Manuscript received April 3, 2006. This work is supported in part by the NIH Grant R01-058856.

H. Zhu, J. Shih, D. S. Long, and M. H. Friedman are with the Department of Biomedical Engineering, Duke University, Durham, NC 27708-0281 USA (phone: 919-660-5225; fax: 919-684-4488; e-mail: hzhu@duke.edu).

N. Maeda, and J. R. Hagaman are with the Department of Pathology and Laboratory Medicine, University of North Carolina at Chapel Hill, Chapel Hill, NC 27599 USA.

II. Materials

Aortic casts were made in two strains of mice (C57BL6 and SVEV) using Batson's No. 17 Plastic Replica and Corrosion Kit from Polysciences, Inc. Final perfusion volumes were scaled down to 2.0 ml per mouse. Immediately following a lethal dose of avertin, the aorta of each mouse was catheterized with MRE 025 tubing (Braintree, Inc) just proximal to the iliac bifurcation. The mouse was then perfused, first with 3 ml heparanized saline (40 unit/ml), and then by freshly prepared casting material until approximately 1.0-1.5 ml had been infused over approximately 4-5 minutes. A small puncture of the vena cava allowed draining of the vascular bed and exit of excess casting material. Carcasses were placed at 4°C overnight and subsequently placed in a maceration solution (saturated KOH) at 37°C with frequent volume changes to clear surrounding tissue (24-48 hrs). Small branches were trimmed with only the aorta and major branches remaining for imaging. Fig.1 shows a C57BL6 cast.

III. Methods

A. Stereo-microscopic Imaging System

The imaging system is based on a Nikon SMZ1000 stereomicroscope (Nikon Instruments, Melville, NY) with a 0.5X objective, a dual beam splitter, a fiber-optic light source (Schott KL 2500 LCD, Schott, Marlborough, MA) (Fig. 2). With different lens adapters, either two Nikon Coolpix 3-million-pixel digital cameras (for color and high spatial resolution), or two PCO 1600 high-performance digital CCD cameras (The Cooke Corporation, Romulus, MI) (for high frame rate) can be mounted on the dual beam splitter to capture stereo images. By either camera setting, the captured images are stored on the camera's flash memory cards or internal memory, and downloaded to a computer through USB or *IEEE* 1394 cables.

Fig. 2. The stereo-microscopic imaging system.

B. Image Acquisition and Imaging System Calibration

The imaging procedure is analogous to that used in our biplane angiographic studies of human coronary arteries [17]. Casts are put in the orientation such that the arch part is approximately perpendicular to the epiploar lines in the view of the microscope (Fig. 5d). This way will benefit the accuracy of the 3-D reconstruction. To facilitate the processing, the light is adjusted properly so that there is high contrast between the cast and the background in the image (Fig. 5a). After capturing the vascular cast images, a calibration device (Fig. 3), which contains fifteen drilled round markers in known relation to one another, is imaged in approximately the location of the cast without disturbing the microscope.

From the theory of computer vision, a projection of a given 3-D point onto a 2-D plane can be represented by the transformation:

$$\begin{pmatrix} u \\ v \end{pmatrix} = \mathbf{T}(x, y, z) = \begin{pmatrix} \dfrac{c_{11}x + c_{12}y + c_{13}z + c_{14}}{c_{31}x + c_{32}y + c_{33}z + c_{34}} \\ \dfrac{c_{21}x + c_{22}y + c_{23}z + c_{24}}{c_{31}x + c_{32}y + c_{33}z + c_{34}} \end{pmatrix} \qquad (1)$$

where (x, y, z) is the coordinate of the point in 3-D space, and (u, v) is its 2-D coordinate in the projection plane. The coefficient vector $\mathbf{c}=(c_{11}, c_{12},\ldots, c_{34})'$ is solved by the normalized Direct Linear Transformation (DLT) algorithm when more than six non-coplanar markers of the calibration cube are located in the projected image, given a usual constraint $\|\mathbf{c}\|=1$ to avoid the solution $\mathbf{c}=0$, which is of no interest [18]. For the stereo views, there are two projection transformations, $\mathbf{T}_L$ and $\mathbf{T}_R$, which have the same format as (1). In our application, the accurate 3-D positions of the markers relative to a bottom corner of the calibration device were measured by a 3-D coordinate measuring machine. The 2-D positions of these markers in an image are located by detecting circles using Hough transform techniques (Fig. 4) [19].

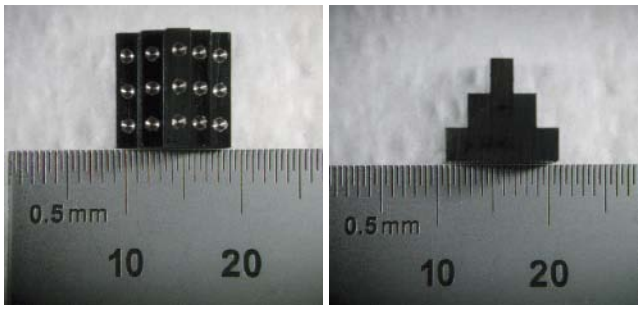

Fig. 3. Top and side views of the calibration device.

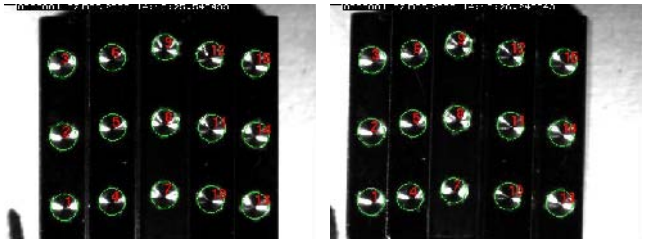

Fig. 4. The round markers detected in the two stereo images of the calibration device.

C. 3-D Axis Reconstruction

The 3-D reconstruction algorithm for a cast axis is a modification of our method to reconstruct 3-D coronary arteries from biplane angiograms [17]. The main change is the image features used to locate the vessel axis due to the different imaging modality used here.

Since we cannot assume that the vessel axis lies along the intensity valleys in an image, which is reasonable for X-ray angiograms, we use the object medialness information here to locate the cast axis under lighting microscope. There are several ways to extract medialness features in an image. We adopted the one proposed by Lopez *et al* [20]. This method can greatly enhance the centerlines of objects in an image using a divergence filter (Fig. 5b).

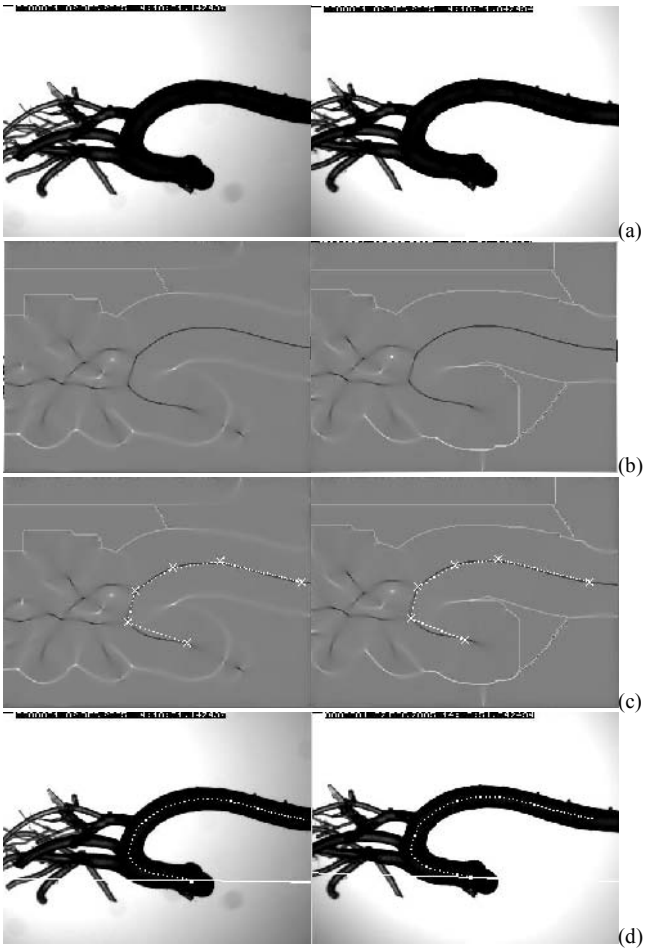

Fig. 5. (a) Two stereo images of an aortic cast. (b) The extracted medialness. (c) Initial plan of the cast axis. (d) Finally located axis projected on the two original images, with the epipolar lines for first point.

With two stereo cast images, several points along the axis of the cast are roughly marked in one image at first. Then, using the two calibration matrices obtained through the calibration device, these points are paired with the corresponding points in the other image by epipolar lines. Each point pair represents the projections of the same 3-D "source" point. The 3-D locations of these source points are reconstructed, and they are initially connected by straight lines as an initial estimate of the 3-D cast axis (Fig. 5c). Finally, this initial 3-D curve is refined to the real axis location by minimizing an energy function, which consists of two forces that arise from the object medialness in the two images (Fig. 5d). The 3-D curve is affected by the two forces through the two calibration matrices.

D. Geometry-based Definition of the Aortic Arch Segment

In the anatomy, a mouse aorta has three segments: ascending aorta, aortic arch, and descending aorta. There is no exact definition which part is the arch area. In the cardiovascular disease study, the aortic arch normally refers to an extended segment, which consists of the most part of the ascending aorta, the aortic arch, and a proximal part of the descending aorta. It is noticed that the major part of the descending aorta is approximately in line-shape. Therefore, to extract the aortic arch segment, we execute the following three steps:

1. Separate the straight part of the descending aorta from the 3-D cast axis. This is achieved by searching for the separation point farthest along the axis from the curve's descending end, which still keeps this portion of the axis well fitted by a line. In other words, the line fitting error is smaller than a threshold;
2. Fit the rest (curved part) of the 3-D cast axis with a plane. This plane is designated as the *x*-*y* plane of a new coordinate system. The *z*-axis of the new coordinate system is perpendicular to this plane. The coordinates' origin is the separation point obtained in step 1 projected to the *x*-*y* plane along the *z* direction. The *y*-axis is the projection of the line fitted to the straight part of the descending aorta. With the *y*-axis, the *x*-axis is easily generated;
3. Transform the 3-D axis curve to the new coordinate system. The aortic arch is defined as the portion of the cast axis above the *x*-*z* plane.

E. Geometric Features

We have studied two local features and a global feature of the mouse aortic arches. The two local features, which are calculated for each point on the curve, are curvature and torsion:

$$\kappa = \left(\frac{(y'z''-y''z')^2 + (z'x''-z''x')^2 + (x'y''-x''y')^2}{\left(x'^2+y'^2+z'^2\right)^3} \right)^{1/2} \quad (2)$$

$$\tau = \frac{abs\left(\begin{vmatrix} x' & y' & z' \\ x'' & y'' & z'' \\ x''' & y''' & z''' \end{vmatrix} \right)}{(y'z''-y''z')^2 + (z'x''-z''x')^2 + (x'y''-x''y')^2} \quad (3)$$

Since all of the casts can be rotated to the same orientation by the above coordinate transformation, we can also compare aortic arch shape globally. We studied the symmetry of the aortic arch using the concept of skewness in statistics:

$$Skewness = \frac{E(x-\mu)^3}{\sigma^3} \quad (4)$$

IV. Results

Fig. 6 shows the top, front and side views of two 3-D reconstructed casts, a C57BL6 and a SVEV. The casts are transformed to the standard orientation described above. The curvatures and torsions of the axes of these two aortic arches are presented in Fig. 7. From the results we can see that while there is only one major curvature peak along the C57BL6 cast axis, two major curvature peaks appear along the SVEV cast axis. Furthermore, both the curvature and torsion of the SVEV's aortic arch are more symmetrical. This is verified by calculating the skewnesses of the two aortic arch segments in their best fitted projection planes, which are 0.20 and -0.03 for the C57BL6 and the SVEV respectively.

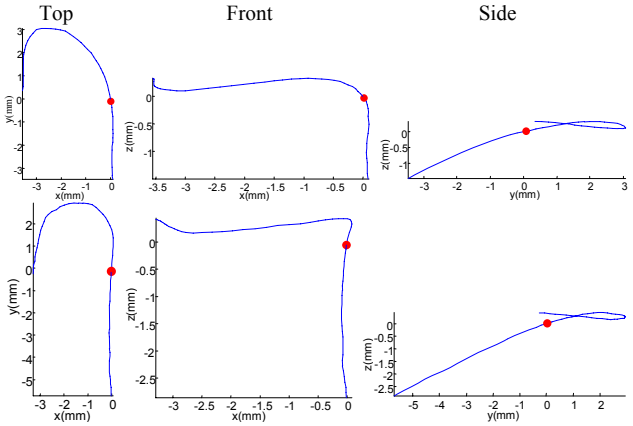

Fig. 6. Top, front, and side views of two aortic arch casts: a C57BL6 (top row) and a SVEV (bottom row). The dots indicate the separation point of the arch segment and the remaining descending aorta.

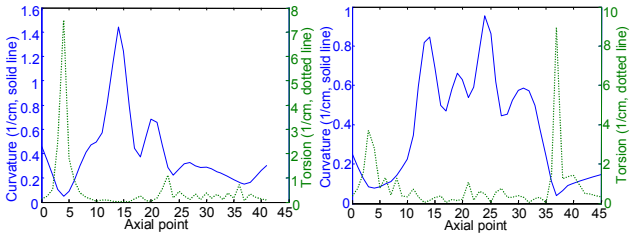

Fig. 7. Curvature and torsion along the axes of the two mouse aortic arches shown in Fig. 6: C57BL6 (left) and SVEV (right). The solid lines are the curvatures, and the dotted lines are the torsions.

V. Conclusion

In this paper, we have proposed a method to study geometric features of mouse aortic arches based on reconstruction of casts using lighting stereo-microscopic imaging. The 3-D vessel axes are transformed to a standard orientation, based on which a geometry-based definition of the aortic arch segment is proposed for the convenience of the comparison study. Some geometric features are compared between the aortic arches of a C57BL6 and a SVEV mouse. The SVEV mouse demonstrates a more symmetrical shape than the C57BL6. More cases are under processing to verify this difference. Further research will include calculation of hemodynamics using the 3-D geometry of the aortic arches, and relate the geometry and hemodynamics to the disease.

References

[1] D. L. Hoyert, M. Heron, S. L. Murphy, and H. C. Kung, "Deaths: Final Data for 2003," Health E-Stats., The National Center for Health Statistics. Released January 19, 2006. Available: http://www.cdc.gov/nchs/products/pubs/pubd/hestats/finaldeaths03/finaldeaths03.htm.

[2] M. H. Friedman, O. J. Deters, F. F. Mark, C. B. Bargeron, and G. M. Hutchins, "Arterial Geometry Affects Hemodynamics - a Potential Risk Factor for Atherosclerosis," *Atherosclerosis*, vol. 46, pp. 225-231, 1983.

[3] Y. Yoshida, T. Yamaguchi, C. G. Caro, S. Glagov, and R. M. Nerem, *Role of Blood Flow in Atherogenesis*. Tokyo: Springer-Verlag, 1988.

[4] D. P. Giddens, C. K. Zarins, and S. Glagov, "The Role of Fluid-Mechanics in the Localization and Detection of Atherosclerosis," *Journal of Biomechanical Engineering-Transactions of the Asme*, vol. 115, pp. 588-594, 1993.

[5] Y. C. Fung, *Biomechanics: circulation*, 2nd ed. New York: Springer, 1997.

[6] M. Narayanaswamy, K. C. Wright, and K. Kandarpa, "Animal models for atherosclerosis, restenosis, and endovascular graft research," *Journal of Vascular and Interventional Radiology*, vol. 11, pp. 5-17, 2000.

[7] A. Daugherty, "Mouse models of atherosclerosis," *American Journal of the Medical Sciences*, vol. 323, pp. 3-10, 2002.

[8] A. Daugherty and D. L. Rateri, "Development of experimental designs for atherosclerosis studies in mice," *Methods*, vol. 36, pp. 129-138, 2005.

[9] R. G. Weiss, "Imaging the murine cardiovascular system with magnetic resonance," *Circulation Research*, vol. 88, pp. 550-551, 2001.

[10] T. Yamashita, S. Kawashima, M. Ozaki, M. Namiki, M. Shinohara, N. Inoue, K. Hirata, K. Umetani, and M. Yokoyama, "In vivo angiographic detection of vascular lesions in apolipoprotein E-knockout mice using a synchrotron radiation microangiography system," *Circulation Journal*, vol. 66, pp. 1057-1059, 2002.

[11] M. D. Lin, C. T. Badea, and G. A. Johnson, "Optimized radiographic spectra for digital subtraction angiography in the mouse," in *Proc. 2004 IEEE International Symposium on Biomedical Imaging: From Nano to Macro*, Arlington, VA, 2004, pp. 1142-1145.

[12] H. W. Schreier, D. Garcia, and M. A. Sutton, "Advances in light microscope stereo vision," *Experimental Mechanics*, vol. 44, pp. 278-288, 2004.

[13] T. Saito, M. Misaki, K. Shirato, and T. Takishima, "3-Dimensional Quantitative Coronary Angiography," *Ieee Transactions On Biomedical Engineering*, vol. 37, pp. 768-777, 1990.

[14] N. Guggenheim, P. A. Doriot, P. A. Dorsaz, P. Descouts, and W. Rutishauser, "Spatial Reconstruction of Coronary-Arteries from Angiographic Images," *Physics in Medicine and Biology*, vol. 36, pp. 99-110, 1991.

[15] A. Wahle, H. Oswald, and E. Fleck, "3D heart-vessel reconstruction from biplane angiograms," *IEEE Computer Graphics and Applications*, vol. 16, pp. 65-73, 1996.

[16] N. E. Green, S. Y. J. Chen, J. C. Messenger, B. M. Groves, and J. D. Carroll, "Three-dimensional vascular angiography," *Current Problems In Cardiology*, vol. 29, pp. 104-142, 2004.

[17] H. Zhu and M. H. Friedman, "Tracking 3-D coronary artery motion with biplane angiography," in *Proc. 2002 IEEE International Symposium on Biomedical Imaging: From Nano to Macro*, Arlington, VA, 2002, pp. 605-608.

[18] R. Hartley and A. Zisserman, *Multiple view geometry in computer vision*, 2nd ed. Cambridge; New York: Cambridge University Press, 2003.

[19] M. Sonka, V. Hlavac, and R. Boyle, *Image processing, analysis, and machine vision*, 2nd ed. Pacific Grove, CA: PWS Pub., 1999.

[20] A. M. Lopez, D. Lloret, J. Serrat, and J. J. Villanueva, "Multilocal creaseness based on the level-set extrinsic curvature," *Computer Vision and Image Understanding*, vol. 77, pp. 111-144, 2000.